ACS APPLIED MATERIALS & INTERFACES

Research Article

www.acsami.org

Photocytotoxicity and Magnetic Relaxivity Responses of Dual-Porous γ-Fe_2O_3@*meso*-SiO_2 Microspheres

Shou-hu Xuan,[†,‡] Siu-Fung Lee,[†] Janet Ting-Fong Lau,[†] Xiaoming Zhu,[†,§] Yi-Xiang J. Wang,[§] Feng Wang,[†] Josie M. Y. Lai,[⊥] Kathy W. Y. Sham,[⊥] Pui-Chi Lo,[†] Jimmy C. Yu,[†] Christopher H. K. Cheng,[⊥] and Ken Cham-Fai Leung*[,†,#]

[†]Institute of Molecular Functional Materials and Department of Chemistry, [§]Department of Imaging and Interventional Radiology, Prince of Wales Hospital, and [⊥]School of Biomedical Sciences, The Chinese University of Hong Kong, Shatin, NT, Hong Kong SAR

[‡]CAS Key Laboratory of Mechanical Behavior and Design of Materials, Department of Modern Mechanics, University of Science and Technology of China, Hefei, 230026, P. R. China

[#]Institute of Creativity and Department of Chemistry, The Hong Kong Baptist University, Kowloon Tong, Kowloon, Hong Kong SAR

Supporting Information

ABSTRACT: Novel high magnetization microspheres with porous γ-Fe_2O_3 core and porous SiO_2 shell were synthesized using a templating method, whereas the size of the magnetic core and the thickness of the porous shell can be controlled by tuning the experimental parameters. By way of an example, as-prepared γ-Fe_2O_3@*meso*-SiO_2 microspheres (170 nm) display excellent water-dispersity and show photonic characteristics under externally applied a magnetic field. The magnetic property of the γ-Fe_2O_3 porous core enables the microspheres to be used as a contrast agent in magnetic resonance imaging with a high r_2 (76.5 s^{-1} mM^{-1} Fe) relaxivity. The biocompatible composites possess a large BET surface area (222.3 m^2/g), demonstrating that they can be used as a bifunctional agent for both MRI and drug carrier. Because of the high substrate loading of the magnetic, dual-porous materials, only a low dosage of the substrate will be acquired for potential practical applications. Hydrophobic zinc(II) phthalocyanine (ZnPC) photosensitizing molecules have been encapsulated into the dual-porous microspheres to form γ-Fe_2O_3@*meso*-SiO_2−ZnPC microspheres. Biosafety, cellular uptake in HT29 cells, and in vitro MRI of these nanoparticles have been demonstrated. Photocytotoxicity (λ > 610 nm) of the HT29 cells uptaken with γ-Fe_2O_3@*meso*-SiO_2−ZnPC microspheres has been demonstrated for 20 min illumination.

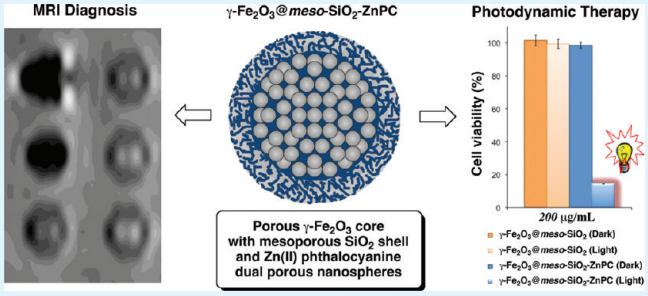

KEYWORDS: *drug carrier, magnetic resonance imaging, nanoparticle, photocytotoxicity, porosity*

1. INTRODUCTION

Colloidal nanoparticles with porous nanostructure have attracted increasing attention with their potential applications in catalysis, separation, sensors, biomedical imaging, diagnosis and therapy due to their high surface areas, well-defined pore structures, as well as tunable particle and pore sizes.[1−7] In view of their applications in cell imaging and drug delivery, recently, combination of mesoporous nanoparticles with other materials together to form multifunctional nanomedical platforms for imaging, diagnosis, and therapy has become a hot research.[8−18] Magnetic iron oxide nanomaterials (Fe_3O_4 and γ-Fe_2O_3) are of great interest for drug delivery[19−27] because they can carry drug molecules and be magnetically guided to the targeted organs or lesion sites inside the body, which will facilitate the therapeutic effect and avoid the damage of normal organs or tissues due to the drug toxicity before targeting the desired positions. Specifically, magnetic nano/microparticles can be used not only as a T_2 contrast agent in magnetic resonance imaging (MRI) but also a magnetically controlled hyperthermia agent, which enable them wildly used in diagnosis and therapy (theranostics).[28−30] Therefore, the integration of noncytotoxic mesoporous silica with magnetic materials to form core/shell nano/microcomposites exhibit great potential for simultaneous MRI, hyperthermia treatment, and drug delivery.[31,32]

In view of biological applications, magnetic core/shell microspheres which possess a uniform particle size below 200 nm, high magnetization, and high colloidal stability in a physiological environment, would be the ideal materials.[33] In the past decade, various candidates such as, Fe_3O_4@SiO_2@*meso*-SiO_2, Fe_3O_4@*meso*-SiO_2, Fe_3O_4@Zeolite, Fe_3O_4@Layered Double Hydroxide, and yolk-like Fe_3O_4@*meso*-SiO_2[31,34−39] core/shell microspheres were developed. However, the sizes

Received: January 2, 2012
Accepted: March 12, 2012
Published: March 12, 2012

   dx.doi.org/10.1021/am300008x | ACS Appl. Mater. Interfaces 2012, 4, 2033−2040

of these materials were larger than 200 nm, which limit their applications for targeted drug delivery, because bigger particles result in more rapidly uptaken by the reticuloendothelial system, such as liver and spleen, leading to a short blood circulation.[40] To solve this problem, recently, Hyeon and coworkers reported the fabrication of magnetic fluorescent delivery vehicle (150 nm) using uniform mesoporous silica spheres embedded monodispersed magnetic and semiconductor nanocrystals.[41] On the basis of that work, they further fabricated discrete, monodisperse core/shell mesoporous silica nanospheres smaller than 100 nm by using single Fe_3O_4 nanocrystals as cores.[33] The sizes of Fe_3O_4@*meso*-SiO_2 can be precisely controlled from 45 to 105 nm, by varying the Fe_3O_4 core concentrations during the formation of the mesoporous silica shell, which enable their bioapplications for simultaneous magnetic resonance and for drug delivery. However, because of the low amount of magnetic nanocrystals encapsulated in the silica particles, their saturated magnetization values were found to be low (<2 emu/g). Obviously, a too small magnetization will weaken the magnetic response of these tiny particles for magnetic separation or targeted drug delivery.[42] Moreover, the low loading of Fe_3O_4 often leads to a high dosage of nanocomposite for MRI. Recently, Zhang et al. reported[43] a modified method to synthesize Fe_3O_4@*meso*-SiO_2 with higher magnetization by increasing the amount of Fe_3O_4 core, however, the magnetic saturations are still smaller than 10 emu/g. In addition, the as-prepared particles should be well-dispersed in physiological environment to allow a long blood half-life, whereas many of present products are not discrete but aggregated. Therefore, it is highly desirable and significant to prepare uniform magnetic *meso*-SiO_2 core/shell nanocomposites with a uniform and tunable small size, high magnetization value, and water-soluble nature for drug delivery.

Herein, we report the fabrication of uniform porous γ-Fe_2O_3 and mesoporous SiO_2,[44] so-called "dual-porous" γ-Fe_2O_3@*meso*-SiO_2 composites that possess core/shell structures with whole particle sizes below 180 nm. In particular, the size of the porous γ-Fe_2O_3 nano/microparticle core and the thickness of the *meso*-SiO_2 shell can be controlled by varying selected experimental parameters. The magnetic core in the nanocomposites renders magnetization and relaxivity properties for MRI. Because of their unique dual-porous nanostructures, the products possess large surface areas. They can be well-dispersed in aqueous solution with photonic characteristics under externally applied magnetic field. In addition, photosensitizing molecules—zinc(II) phthalocyanine (ZnPC)—were loaded to the dual-porous γ-Fe_2O_3@*meso*-SiO_2 to form γ-Fe_2O_3@*meso*-SiO_2−ZnPC composite microspheres. Phthalocyanine and porphyrin compounds are excellent candidates for photodynamic therapy (PDT).[45,46]

2. EXPERIMENTAL SECTION

Materials. Ferric chloride hexahydrate ($FeCl_3{\cdot}6H_2O$), sodium acetate (NaOAc), ethylene glycol (EG), diethylene glycol (DEG), poly(acrylic acid) (PAA, M_w = 1.8 kDa), tetraethyl orthosilicate (TEOS), and octadecyltrimethoxysilane (C_{18}TMS) were obtained from Aldrich. All chemicals were of analytical grade and used without further purification. Deionized water was obtained from Barnstead RO pure system and was bubbled with high-purity nitrogen for at least 30 min before use.

Synthesis of Monodispersed γ-Fe_2O_3@*meso*-SiO_2. First, the Fe_3O_4 with variable particle sizes were synthesized according to our previous reports.[29,47] The Fe_3O_4 nano/microparticles were dispersed in ethanol (30 mL) under sonication. After 10 min, H_2O (3 mL) and ammonia (1 mL) were added to the above solution. After an hour, a mixture of TEOS (0.225 mL) and C_{18}TMS (0.075 mL) in ethanol (5 mL) was added into the system. After 3 h, the Fe_3O_4@*hybrid*-SiO_2 product was collected by centrifugation, washed with ethanol twice, and then dried in vacuum for 12 h. Then, the Fe_3O_4@*hybrid*-SiO_2 microspheres were heated in vacuum from ambient temperature to 550 °C at a heating rate of 5 °C/min. After 6 h thermo-treatment at 550 °C, the product was cooled down to room temperature and further heated in air at 250 °C for another 6 h. Then, the product was cooled as well as rinsed with diluted ammonia solution, H_2O, and ethanol under magnetic separation. After a drying process, the dual-porous γ-Fe_2O_3@*meso*-SiO_2 microspheres were obtained.

Synthesis of γ-Fe_2O_3@*meso*-SiO_2−ZnPC. Dual-porous γ-Fe_2O_3@*meso*-SiO_2 microspheres were soaked in a saturated solution of zinc(II) phthalocyanine (ZnPC) in DMF for 24 h and then magnetically separated. The amount of ZnPC adsorbed into the 170 nm dual-porous γ-Fe_2O_3@*meso*-SiO_2 microspheres was approximately 10 mg (to 50 mg in supersaturated state through continuous evaporation) ZnPC per gram of porous microspheres. The absorbed amount of ZnPC to the microspheres was determined by their UV absorption signal intensity before and after the addition. The γ-Fe_2O_3@*meso*-SiO_2−ZnPC microspheres were soaked in phosphate buffer saline (PBS) for 2 h without degradation and release of ZnPC unless with the presence of ethanol.

Characterization. Transmission electron microscopy (TEM) photographs were taken on a FEI CM120 microscope at an accelerating voltage of 120 kV and a high-resolution transmission electron microscope (HRTEM, Tecnai F20, FEI) at an accelerating voltage of 200 kV. The general morphology of the product was characterized by scanning electron microscopy (SEM, FEI Quanta 400 FEG microscopes). X-ray powder diffraction patterns (XRD) of the products were obtained on a Bruker D8 Advance diffractometer equipped with graphite monochromatized Cu Kα radiation (λ = 1.5406 Å). Infrared (IR) spectra were recorded in the wavenumbers ranging from 4000 to 500 cm^{-1} with a Nicolet Model 759 Fourier Transform Infrared (FT-IR) spectrometer using a KBr wafer. UV/visible absorption spectra were obtained using a Cary 5G UV/visible/NIR spectrophotometer with a scan rate of 300 nm/min. The magnetic properties (M−H curve) were measured at room temperature on a Lakeshore 7300 magnetometer. Inductively coupled plasma-optical emission spectroscopy (ICP-OES) was performed on Optima 4300 DV ICP-OES. Samples were dissolved in 2% HCl solution with a few drops of $SnCl_2$ solution. Iron absorption was observed at 238.204 nm. The iron contents in a dispersed nanoparticle solution (in terms of g/mL) as well as in each nanoparticle (in terms of %) were determined. The Brunauer−Emmett−Teller (BET) surface areas of the samples were analyzed by nitrogen adsorption−desorption isotherm measurements at 77 K on a nitrogen adsorption apparatus (Micromeritics ASAP 2010). All the samples were degassed at 150 °C prior to the measurements. Pore size distributions were calculated from the desorption branch of the isotherm by the Barrett−Joyner−Halenda (BJH) method using Halsey equation.

Cell Lines and Culture Conditions. The HT29 human colon adenocarcinoma cells (from ATCC, no. HTB-38) were maintained in Dulbecco's modified Eagles' medium (DMEM; Invitrogen, cat no. 10313−021) supplemented with 10% fetal calf serum, 100 units/mL penicillin, 100 mg/mL streptomycin, 2 mM L-glutamine, and 10 mg/mL transferrin. Approximately 3×10^4 cells per well in these media were inoculated in 96-multiwell plates and incubated overnight at 37 °C in a humidified 5% CO_2 atmosphere.[13] MDCK (Madin-Darby Canine Kidney Cells, ATCC CCL-34) were grown in DMEM medium supplemented with FBS (10%), streptomycin (100 μg/mL), penicillin (50 U/mL) at 37 °C in a 5% CO_2 humidified atmosphere.

Cellular Uptake. The cellular uptake of γ-Fe_2O_3@*meso*-SiO_2−ZnPC microspheres was evaluated in HT29 cells by Prussian blue staining and intracellular iron concentration study by ICP-OES. HT29 cells were seeded in a 24-well plate in DMEM medium containing 10% FBS. After 12 h incubation, medium was replaced with serum-free DMEM medium containing different concentrations (0, 5, 10, and 20 μg/mL) of nanocomposite and incubated for another 20 h. At the end

of incubation, cells were washed with PBS for 3 times, and Prussian blue staining or ICP-OES analysis was performed. In Prussian blue staining, cells were fixed for 40 min by using 4% paraformaldehyde. After washing with PBS, the cells were incubated with Perls' reagent (4% potassium ferrocyanide and 6% HCl) for 30 min, and followed by a neutral red counterstain. The cells were observed using a light microscopy. To determine intracellular iron concentration, the cells were collected and counted. Cells were resuspended in 200 μL 12% HCl solution and incubated at 60 °C for 4 h to dissolve the microspheres. $SnCl_2$ was added to convert Fe^{3+} to Fe^{2+}, and the solution was further diluted to 1 mL. Subsequently, ICP-OES was performed to study the iron concentrations before and after nanoparticle incubation with cells.

Photocytotoxicity Assay. The γ-Fe_2O_3@*meso*-SiO_2−ZnPC nanoparticles were first formulated with lipofectamine (Invitrogen, cat no. 18324−020) to give 2000 μg mL^{-1} (1:1 nanoparticle:lipofectamine) solutions. The standard protocols can be found in the literature.[45,46]

Magnetic Resonance Relaxometry. For MRI, standard conditions and parameters can be found in the literature.[48] *In vitro* MRI was performed with HT29 cells labeled with γ-Fe_2O_3@*meso*-SiO_2−ZnPC microspheres (20 μg/mL) for 20 h. After washing with PBS, the cells were trypsinized and counted. Different number (0, 1×10^3, 3×10^3, 6×10^3, 1×10^4, 3×10^4, 6×10^4, 1×10^5, 3×10^5, 6×10^5, 1×10^6 or 3×10^6) of cells was placed in Eppendorf tubes. MRI was performed with a 3.0 T clinical whole-body MR unit. For HT29 cells labeled with γ-Fe_2O_3@*meso*-SiO_2−ZnPC microspheres (20 μg/mL), pellets of ≥1000 cells were detectable by MRI.

3. RESULTS AND DISCUSSION

The synthesis of γ-Fe_2O_3@*meso*-SiO_2 microspheres with tunable sizes is shown in Figure 1. Monodispersed, photonic-grade poly(acrylic acid) (PAA)-entangled Fe_3O_4 microspheres (see Figure S1 in the Supporting Information) with tunable sizes were prepared by using a facile solvothermal synthesis.[29,47] A layer of inorganic−organic hybrid SiO_2 shell that is formed from simultaneous sol−gel polymerization with tetraethyl orthosilicate (TEOS) and octadecyltrimethoxysilane (C_{18}TMS), was deposited on the surface of the PAA-entangled Fe_3O_4 microspheres.[49] This procedure results in the formation of the core/shell Fe_3O_4@*hybrid*-SiO_2 microspheres. Subsequently, the core/shell Fe_3O_4@*hybrid*-SiO_2 microspheres were calcined in vacuum for removal of the organic group which existed both in the core (PAA) and the shell (C_{18} alkyl chain).

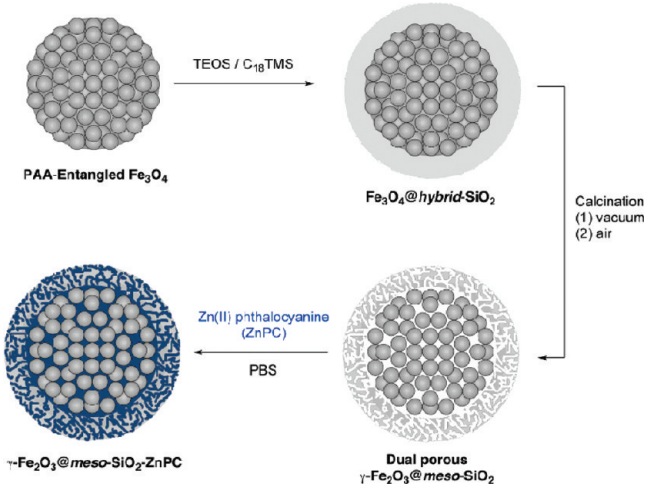

Figure 1. Graphical representation of the synthesis of Fe_3O_4@*hybrid*-SiO_2, dual-porous γ-Fe_2O_3@*meso*-SiO_2, and γ-Fe_2O_3@*meso*-SiO_2−ZnPC microspheres.

The material was further calcined with air first, to transform the Fe_3O_4 core into γ-Fe_2O_3 and second, to decompose any organic residues of the material. Then, the γ-Fe_2O_3@*meso*-SiO_2 microspheres with porous core and porous shell were obtained. Since the size of the Fe_3O_4 microspheres can be tuned from 40 to 200 nm in the above method,[29,47] this process represents a general strategy for the synthesis of uniform dual-porous γ-Fe_2O_3@m-SiO_2 microspheres with tunable core size and shell thickness. For drug loading, the dual-porous γ-Fe_2O_3@*meso*-SiO_2 microspheres were soaked in a concentrated solution of ZnPC and then magnetically separated. The γ-Fe_2O_3@*meso*-SiO_2−ZnPC microspheres were redispersed in phosphate buffer saline (PBS) without any degradation or release of ZnPC, unless with the presence of ethanol.

PAA-entangled Fe_3O_4 microspheres with average diameters of 120 nm (see Figure S2a in the Supporting Information) were used to present the simplicity in the particle synthesis. Through the sol−gel coating and heating treatment, dual-porous γ-Fe_2O_3@*meso*-SiO_2 microspheres were obtained. As shown SEM image in Figure 2a, the products are spherical in shape and

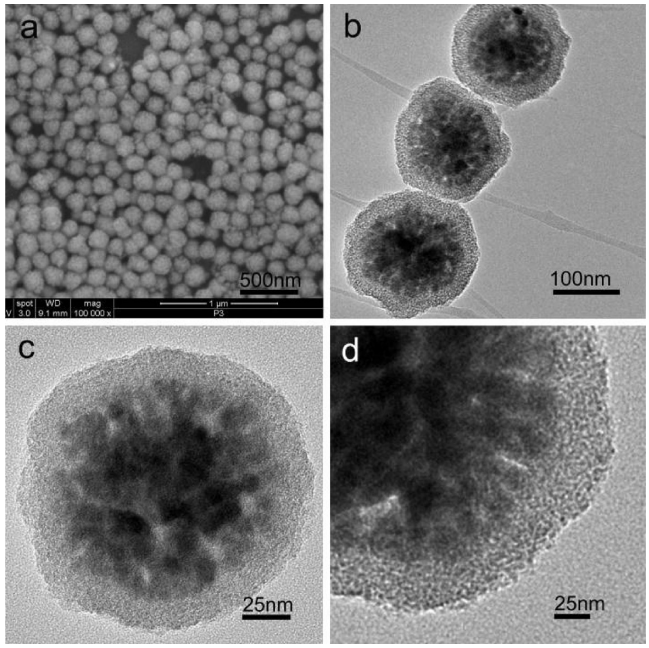

Figure 2. (a) SEM and (b−d) TEM images of 170 nm γ-Fe_2O_3@*meso*-SiO_2 microspheres.

relatively uniform in dimension with particle diameters of ca. 170 nm after a washing process. It can be observed from the image that all the microspheres were well-dispersed without any large aggregations (see Figure S3 in the Supporting Information). These particles exhibit core/shell nanostructure as shown in the TEM images (Figures 2b,c). The diameter of the microspheres is around 170 nm, and this result agrees well with the SEM characterization. The shell of these microspheres, which possess a thickness of about 25 nm, contain framework-confined pores, as revealed by the TEM images (Figure 2d).[50] Clearly, these mesopores are nonordered. It should be noted that the magnetic cores are identified as γ-Fe_2O_3, according to the XRD measurement (see Figure S4 in the Supporting Information). In comparison to the Fe_3O_4 precursor, XRD diffraction peak of the dual-porous γ-Fe_2O_3@*meso*-SiO_2 shifted a few degrees, which suggested the formation of γ-Fe_2O_3

(JCPDF No. 39−1346).[48] In the synthesis, after the heating treatment under air condition, the color of the product transformed from black to brown, also indicating that the Fe_3O_4 core was oxidized to γ-Fe_2O_3.

The textural characteristics of the dual-porous core/shell microspheres were examined by means of the nitrogen sorption isotherm and pore size distribution (Figures 3 and Figures S14

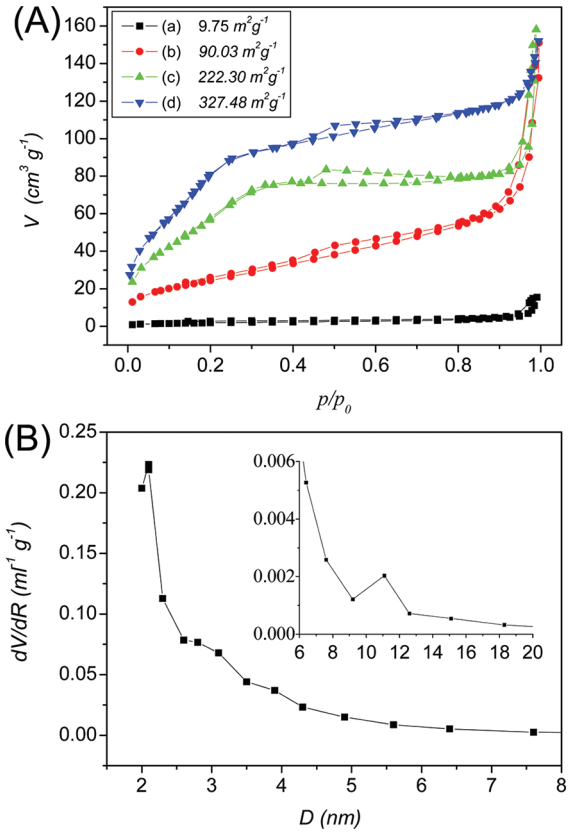

Figure 3. (A) N_2 adsorption/desorption isotherms of (a) nonporous Fe_3O_4*@hybrid*-SiO_2; (b) 120 nm dual-porous γ-Fe_2O_3*@meso*-SiO_2; 170 nm dual-porous γ-Fe_2O_3*@meso*-SiO_2; and (c) 250 nm dual-porous γ-Fe_2O_3*@meso*-SiO_2. (B) Pore size distributions of the 170 nm dual-porous γ-Fe_2O_3*@meso*-SiO_2 microspheres.

in the Supporting Information). Before heating treatment, the as-prepared Fe_3O_4*@hybrid*-SiO_2 that contains the organic $-(CH_2)_{17}$-CH_3 group in the hybrid SiO_2 shell is nonporous, as can be deduced from the nitrogen sorption isotherm shown in Figure 3Aa (S_{BET} = 9.75 m^2/g).[31,32] After calcinations, the resulting γ-Fe_2O_3*@meso*-SiO_2 exhibits a much higher BET surface area of 222.3 m^2/g (Figure 3Ac) due to the dual-porous structure. Two relatively low-intensity hysteresis loops at P/P_0 0.4−0.8 and 0.85−0.98 in the isotherm (Figure 3Ac) were observed, indicating the mesoporous is disordered and they are packed by many small particles.[50] For pore size distributions of the 170 nm dual-porous γ-Fe_2O_3*@meso*-SiO_2 microspheres, the porosity renders (Figure 3B) mesopores in the range of 2−15 nm. Obviously, the maximum centered at 2.1 nm should be attributed to the mesoporous silica shell and other weaker signals of 3.0 and 11.1 nm are corresponded to the porous γ-Fe_2O_3 core.[48]

Our synthetic method was extended to prepare smaller γ-Fe_2O_3*@meso*-SiO_2 microspheres with an average diameter of 120 nm, by starting with the 80 nm PAA-entangled Fe_3O_4 microspheres. *Ca.* 20 nm hybrid silica shell was coated to the 80 nm PAA-entangled Fe_3O_4 microspheres to form the uniform core/shell 120 nm Fe_3O_4*@hybrid*-SiO_2 and the γ-Fe_2O_3*@meso*-SiO_2 microspheres (Figure 4a). TEM images of the 120 nm γ-Fe_2O_3*@meso*-SiO_2 microspheres also reveal (inset of Figure 4a) the framework-confined mesopores of silica shell and voids of γ-Fe_2O_3 core. Using current synthetic method, we were able to control the size of the composite nanosphere simply by varying the size of the Fe_3O_4 core. For example, 250 nm dual-porous magnetic particles were also successfully obtained when the 210 nm Fe_3O_4 microspheres were used as the precursor. Images b and c in Figure 4 show that the peripheral of the 170 and 250 nm γ-Fe_2O_3*@meso*-SiO_2 is brighter than the center, which suggests the core/shell structure of the microspheres. The yield of the core/shell particles is very high.

To understand the formation mechanism, the synthesis procedure for the 250 nm γ-Fe_2O_3*@meso*-SiO_2 is studied by TEM investigation. The initial Fe_3O_4 particles with the average diameters of 210 nm (Figure 4d) were used to present the simplicity of this flexible synthetic route. As shown in Figure 4h, the Fe_3O_4 microsphere, which is composed of Fe_3O_4 nanoparticles with size between 5−10 nm, shows a clusterlike nanostructure.[29] These uniform cores resulted in a narrow distribution of the Fe_3O_4*@hybrid*-SiO_2 particle sizes. The TEM image shows that the hybrid silica coating is also uniform with a thickness of 20 nm (Figures 4e,i). In this case, a mixture of TEOS and C_{18}TMS was used as the hybrid silica precursor. The shell thickness can be tuned by varying the concentration of the silica precursor.[31] Without the C_{18}TMS, only dense SiO_2 shells were obtained. The C_{18}TMS was employed as the surfactant to substitute cetyltrimethylammonium bromide (CTAB) due to the last one often led to aggregation of the Fe_3O_4 particles in present system. TEM images show the Fe_3O_4*@hybrid*-SiO_2 microspheres are of typical core/shell nanostructure (Figure 4e). In comparison to the Fe_3O_4@SiO_2 nanosphere with pure SiO_2 framework hydrolyzed from TEOS (see Figure S5d in the Supporting Information), the Fe_3O_4*@hybrid*-SiO_2 nanosphere exhibits a relatively rough surface (Figures 4i and Figure S5a−c in the Supporting Information), which may respond to the presence of micelle aggregates.[49]

The organic moiety $-(CH_2)_{17}-H_3$ of the organo-silicon compound C_{18}TMS acts as a surfactant, and these organic moieties in the pores could be removed to form *meso*-SiO_2 shell by calcination. Due to the ease of oxidation of Fe_3O_4 and γ-Fe_2O_3 to form α-Fe_2O_3 at high temperature in air or in the presence of oxygen, a two-step calcination method, that is, the treatment of the Fe_3O_4*@hybrid*-SiO_2 with high temperature (550 °C) under vacuum and subsequent heating with relative low temperature (250 °C) under air condition, were conducted to synthesize dual-porous γ-Fe_2O_3*@meso*-SiO_2 microspheres. Obviously, the porosity generated in the dual-porous materials is corresponded to a release of volatile gases produced during pyrolysis of the $-(CH_2)_{17}$-CH_3 group in the hybrid SiO_2 shell and the poly(acrylic acid) in the magnetic core (as proved by the FTIR results in Figure S6 in the Supporting Information). Because the reaction was performed in a vacuum condition, carbon was present in the pore of both the γ-Fe_2O_3 core and *meso*-SiO_2 shell, which can be detected by the Raman spectroscopy (see Figure S7 in the Supporting Information).[51] This phenomenon further explains that why our product show a smaller pore size (2.1 nm) and BET (222.3 m^2/g) as compared to the pure *meso*-SiO_2, which was synthesized by using C_{18}TMS as the surfactant.[52,53] Under a low-temperature

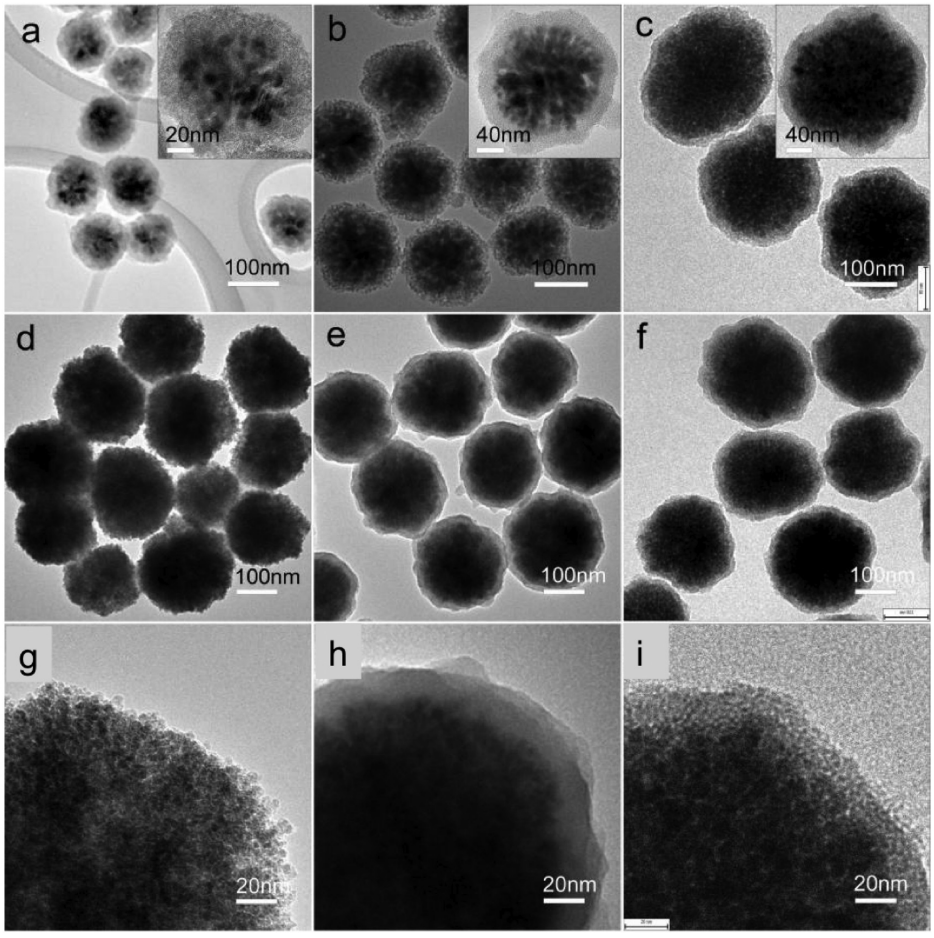

Figure 4. TEM images of γ-Fe_2O_3@*meso*-SiO_2 microspheres with different sizes: (a) 120, (b) 170, and (c, f, i) 250 nm; TEM images of (d, g) Fe_3O_4 and (e, h) Fe_3O_4@*hybrid*-SiO_2 microspheres.

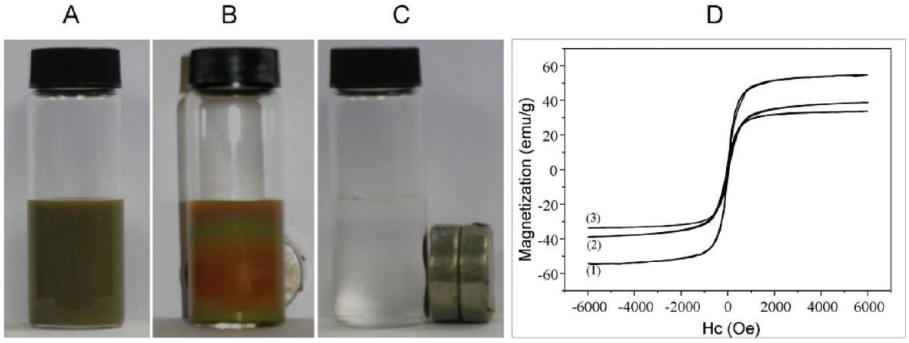

Figure 5. (A–C) Pictures of aqueous dispersion of dual-porous γ-Fe_2O_3@*meso*-SiO_2 microspheres. The relative colloidal crystals (A) formed in response to an external magnetic field (B), and finally separated from the solution (C). (D) Hysteresis loops of 120 nm PAA-entangled Fe_3O_4 microspheres (1), dual-porous γ-Fe_2O_3@*meso*-SiO_2 microspheres with 250 nm (2) and 170 nm (3).

heating treatment in air, partial carbon residues were removed and the Fe_3O_4 cores were transformed into γ-Fe_2O_3, and finally dual-porous γ-Fe_2O_3@*meso*-SiO_2 core/shell microspheres were successfully obtained.

In this procedure, the size of the γ-Fe_2O_3@*meso*-SiO_2 core/shell microspheres and the shell thickness of the *meso*-SiO_2 shell can be precisely controlled by tuning the size of the Fe_3O_4 core and the concentration of the TEOS/C_{18}TMS (see Figure S2d,e in the Supporting Information), respectively, and the BET can be tuned by changing the molar ratio of TEOS/C_{18}TMS, which clearly shows the flexibility of the methodology presented. As shown in Figure S8 in the Supporting Information, 350 nm γ-Fe_2O_3@ core/shell microspheres with 60 nm *meso*-SiO_2 shell thickness can also be obtained. Figures S2 and S9 in the Supporting Information show the TEM images of the 170 and 120 nm Fe_3O_4@*hybrid*-SiO_2, treated with high temperature (550 °C) under vacuum, and subsequent heating with relative low temperature (250 °C) in air, which further confirm the formation mechanism. Here, the BET areas of the γ-Fe_2O_3@m-SiO_2 core/shell microspheres with diameter of 120, 170, and 250 nm are 90, 222, and 327 m^2/g (Figures 3b,c,d), respectively. In addition, the dissolution of the γ-Fe_2O_3

dx.doi.org/10.1021/am300008x | *ACS Appl. Mater. Interfaces* 2012, 4, 2033–2040

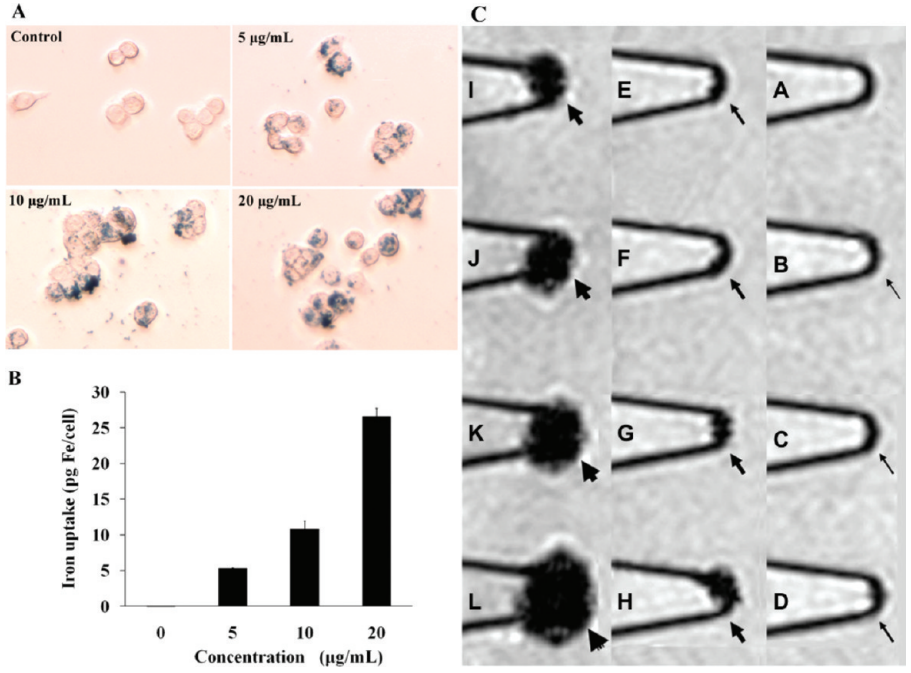

Figure 6. Cellular uptake of γ-Fe_2O_3@*meso*-SiO_2–ZnPC microspheres (5, 10, and 20 μg/mL) in HT29 cells evaluated by Prussian blue staining (A) and intracellular iron concentration study by ICP-OES (B). (C): *In vitro* MRI results. Gradient echo MR images of HT29 cell pellets labeled with γ-Fe_2O_3@meso-SiO_2–ZnPC microspheres (20 μg/mL) in eppendorf tubes with culture medium. The cell number in eppdendorf tubes is (A) 0, (B) 1×10^3, (C) 3×10^3, (D) 6×10^3, (E) 1×10^4, (F) 3×10^4, (G) 6×10^4, (H) 1×10^5, (I) 3×10^5, (J) 6×10^5, (K) 1×10^6, and (L) 3×10^6, respectively.

of the composites gives rise to uniform *meso*-SiO_2 microspheres with a hollow interior, as can be observed from the TEM image (see Figure S2f in the Supporting Information).

Colloidal stability under physiological condition is essential for biomedical applications. The dual-porous γ-Fe_2O_3@*meso*-SiO_2 microspheres could be readily dispersed and magnetic separated (with a relatively long separation time) in H_2O, PBS, and ethanol. The solution is very stable and no distinct precipitation can be found within 10 h. To investigate the magnetic field on the colloidal stability of the microspheres, we placed a piece of magnet near the glass bottle. Interestingly, this solution can diffract visible light upon the external magnetic field as demonstrated in Figure 5B. Obviously, the magnetic particles must be assembled to form colloidal photonic crystals in the magnetic field[54,55] and this reversible optical response phenomenon has not been reported on the previously developed magnetic drug carriers. The magnetization saturation value (M_s) of the 170 nm γ-Fe_2O_3@*meso*-SiO_2 is 32.5 emu/g (Figure 5D3), which is much higher than the previously reported nano/microparticles.[33,41,43] The γ-Fe_2O_3 content of core/shell microspheres is about 55%, indicating a high loading of Fe element. For 250 nm γ-Fe_2O_3@*meso*-SiO_2, the M_s is 39 emu/g (Figure 5D2), which corresponded to their large core size. As a result, the microspheres in their homogeneous dispersion show fast moment to the applied magnetic field to form photonic crystals and be attracted toward the magnet under a relative long separation time (Figure 5C). Moreover, the separated particles can be redispersed quickly with a slight shake once the magnetic field is removed. These results further confirm that as-prepared microspheres, which possess excellent magnetic properties and water redispersibility, can be used to carry drugs to targeted locations under an external magnetic field.

The γ-Fe_2O_3@*meso*-SiO_2 microspheres could be used as diagnostic MRI contrast agent because the magnetic iron oxide core could accelerate the transverse relaxation of water protons.[28−30] Transverse (T_2) relaxation times of protons from the dispersion containing 170 nm γ-Fe_2O_3@*meso*-SiO_2 microspheres were measured (see Figure S10A in the Supporting Information) in various concentrations and that the r_2 relaxivity of the microspheres was determined to be 76.5 $s^{-1}mM^{-1}$ Fe (see Figure S10B in the Supporting Information). However, the determined r_2 relaxivity of the microspheres is smaller than the r_2 relaxivity (120 s^{-1} mM^{-1} Fe) of commercially available MRI contrast agent—Ferumoxides, with a size between 120−180 nm. This is partly because our microspheres contain a thicker outer silica shell.

Because the aim of this work and the success in potential applications depend on the core particle size, shell thickness, and porosity, which are directly related to the superparamagnetivity, magnetic saturation, drug loading amount, cell uptake ability, magnetic relaxivity, and photocytotoxicity. The 170 nm microspheres (among the 250 and 120 nm microspheres) would give us insights on the initial bioevaluation for future detailed investigation of drug loading and size-property relationships in different sized nano/microspheres. To demonstrate the applicability of this dual-porous magnetic system, we employed the 170 nm γ-Fe_2O_3@*meso*-SiO_2 microspheres as a drug carrier and Zinc(II) phthalocyanine (ZnPC) as the model drug. The porous microspheres were soaked in a concentrated solution of ZnPC in DMF (1 M) for 24 h and separated by a magnet. The amount of ZnPC adsorbed into the porous materials was about 53 mg/g, which was obtained from the UV absorbance difference before the addition and removal of the microspheres, as shown in Figure S11a in the Supporting Information. The successful loading of the ZnPC can be confirmed further by the FTIR and UV/

visible spectra (see Figure S11b,c in the Supporting Information). The microspheres loaded with ZnPC were soaked in phosphate buffered saline (PBS) solution for 2 h and then magnetic separated and the supernatants were measured (in Figure S11c in the Supporting Information), which show that ZnPC was retained in the porous materials when incubated in PBS, whereas it will release out from the mesoporous in the presence of ethanol. Indeed, it has been experimentally observed that ZnPC loaded γ-Fe_2O_3@*meso*-SiO_2 microspheres dispersed in a buffer solution are attracted by a conventional magnet placed close to the vessel, a clear demonstration of the potential of magnetic targeting drug delivery.

We employed Prussian blue staining to demonstrate that γ-Fe_2O_3@*meso*-SiO_2–ZnPC microspheres could be internalized by HT29 human colorectoral carcinoma cells. After staining, the dense blue stained dots could be clearly observed (Figure 6A) in HT29 cytoplasm under optical microscope, as shown in the typical images of HT29 cells treated with microspheres 5, 10, or 20 μg/mL. Subsequently, ICP-OES assay was employed to evaluate quantitatively the cellular uptake of the microspheres. As shown in Figure 6B, the iron content in HT29 cells significantly increased with the concentration of the microspheres. Each γ-Fe_2O_3@*meso*-SiO_2–ZnPC nanosphere possessed an average 52% (weight %) of iron. In particular, the nanosphere concentration of 0, 5, 10, and 20 μg/mL rendered 0, 5.4, 11.9, and 27.1 pg Fe/cell, respectively. In vitro MRI (Figure 6C) was performed with HT29 cells labeled with γ-Fe_2O_3@*meso*-SiO_2–ZnPC microspheres (20 μg/mL) for 20 h. After washing with PBS, the cells were trypsinized and counted. Different number of cells were placed in eppendorf tubes. Pellets of $\geq$1000 cells were detectable by MRI.

Madin-Darby Canine Kidney Cells (ATCC CCL-3) were incubated with the microspheres to evaluate the particle's biocompatibilities, with MTT assay (see Figure S12 in the Supporting Information). It revealed that cell viabilities were not hindered following culture with 10 μg of Fe_3O_4 and γ-Fe_2O_3@*meso*-SiO_2 microspheres. In comparison to lipofectamine (positive control), they exhibit lower cytotoxicities, which indicate that the Fe_3O_4 and γ-Fe_2O_3@*meso*-SiO_2 microspheres are biocompatible. To demonstrate that the as-synthesized γ-Fe_2O_3@*meso*-SiO_2–ZnPC composite microspheres are promising materials for theranostic purposes with PDT properties, reactive oxygen species (e.g., singlet oxygen) should be generated upon red light (λ > 610 nm) irradiation of the trapped photosensitizing ZnPC molecules.[45,46,56] The in vitro photodynamic activities of 170 nm γ-Fe_2O_3@*meso*-SiO_2 and 170 nm γ-Fe_2O_3@*meso*-SiO_2–ZnPC in lipofectamine emulsions were investigated against HT29 human colorectoral carcinoma cells as shown in Figure 7. Both microspheres were noncytotoxic up to 200 μg/mL in the absence of light. Upon illumination, the γ-Fe_2O_3@*meso*-SiO_2–ZnPC exhibited high photocytotoxicity, whereas 170 nm γ-Fe_2O_3@*meso*-SiO_2 was noncytotoxic. The cell viability was reduced to 10% after incubation with γ-Fe_2O_3@*meso*-SiO_2–ZnPC (200 μg/mL) for 20 h and illumination. A controlled release of ZnPC molecules from the pores of the composite microspheres may not be necessary to facilitate the therapeutic purpose because reactive oxygen species may effectively diffuse out from the pores to generate photocytotoxicity. Evidently, the γ-Fe_2O_3@*meso*-SiO_2–ZnPC composite nanosphere itself acts as a theranostic agent.

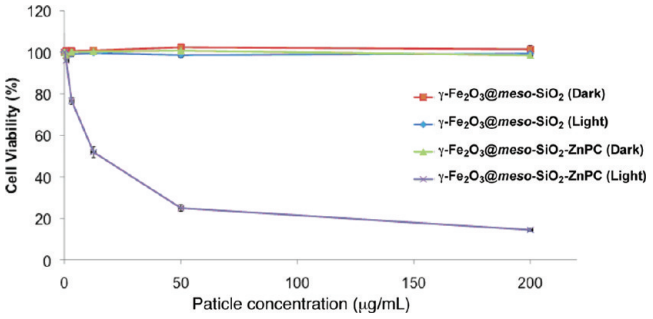

Figure 7. Comparison of the cytotoxic effects of 170 nm γ-Fe_2O_3@*meso*-SiO_2 and 170 nm γ-Fe_2O_3@*meso*-SiO_2–ZnPC on HT29 cells in the absence and presence of light (λ > 610 nm, 40 mW cm^{-2}, 48 J cm^{-2}) for 20 min illumination.

4. CONCLUSION

In conclusion, a series of novel dual-porous γ-Fe_2O_3@*meso*-SiO_2–ZnPC microspheres has been developed and investigated with their particle sizes, shell thickness, porosities, and magnetization values (see Table S1 in the Supporting Information). In addition, by way of an example, as-prepared γ-Fe_2O_3@*meso*-SiO_2 microspheres (170 nm) display a high r_2 (76.5 $s^{-1}mM^{-1}$ Fe) relaxivity. Generally, the composite microspheres possess large BET surface areas (90–327 m^2/g), demonstrating that they can be used as a bifunctional agent for both MRI and drug carrier. Photosensitizing zinc(II) phthalocyanine molecules have been encapsulated into the dual-porous microspheres to form γ-Fe_2O_3@*meso*-SiO_2–ZnPC microspheres. Biosafety, cellular uptake in HT29 cells, and in vitro MRI of these nanoparticles have been demonstrated. Photocytotoxicity (λ > 610 nm) of the HT29 cells uptaken with γ-Fe_2O_3@*meso*-SiO_2–ZnPC microspheres has been demonstrated for 20 min illumination. For applications,[57] Fe_3O_4 nanoparticles are used to help cancer diagnosis and staging, clinically, these particles of larger size (80–150 nm) are used for liver cancer characterization.[58] The uptake of intravenously administered silica-coated nanoparticles,[59–61] nanowires,[62] and hollow nanostructures[63] by phagocytic monocytes and macrophages also provides a valuable in vivo tool by which MRI can be used to monitor involvement of macrophages in inflammatory processes, such as multiple sclerosis, traumatic nerve injury, stroke, and brain tumors.

■ ASSOCIATED CONTENT

Ⓢ Supporting Information

Additional TEM and MRI images, XRD, FTIR, Raman, UV/visible spectra, cell viability data, porosity data, and summary table. This material is available free of charge via the Internet at http://pubs.acs.org.

■ AUTHOR INFORMATION

Corresponding Author

*Phone: (+852) 3411 2319. E-mail: cfleung@hkbu.edu.hk.

Notes

The authors declare no competing financial interest.

■ ACKNOWLEDGMENTS

We acknowledge the financial support by RGC-GRF (401709), UGC (AoE/P-03/08) research grants and NSFC (11102202). Mr. Feng Zhao is grafully acknowledged.

REFERENCES

(1) Chen, H. R.; Shi, J. L.; Li, Y. S.; Yan, J. N.; Hua, Z. L.; Chen, H. G.; Yan, D. S. *Adv. Mater.* **2003**, *15*, 1078−1081.
(2) Yu, C.; Fan, J.; Tian, B.; Zhao, D. *Chem. Mater.* **2004**, *16*, 889−898.
(3) Yamada, T.; Zhou, H.; Honma, I.; Katsube, T. *J. Phys. Chem. B* **2004**, *108*, 13341−13346.
(4) Kim, J.; Piao, Y.; Hyeon, T. *Chem. Soc. Rev.* **2009**, *38*, 372−390.
(5) Piao, Y.; Burns, A.; Kim, J.; Wiesner, U.; Hyeon, T. *Adv. Funct. Mater.* **2008**, *18*, 3745−3758.
(6) Liong, M.; Angelos, S.; Choi, E.; Patel, K.; Stoddart, J. F.; Zink, J. I. *J. Mater. Chem.* **2009**, *19*, 6251−6257.
(7) Lim, J.; Lee, S. S.; Ying, J. Y. *Chem. Commun.* **2010**, *46*, 806−808.
(8) Nasongkla, N.; Bey, E.; Ren, J.; Ai, H.; Khemtong, C.; Guthi, J. S.; Chin, S. F.; Sherry, A. D.; Boothman, D. A.; Gao, J. *Nano Lett.* **2006**, *6*, 2427−2430.
(9) Lee, J. E.; Lee, N.; Kim, H.; Kim, J.; Choi, S. H.; Kim, J. H.; Kim, T.; Song, I. C.; Park, S .P.; Moon, W. K.; Hyeon, T. *J. Am. Chem. Soc.* **2010**, *132*, 552−557.
(10) Rieter, W. J.; Kim, J. S.; Taylor, K. M. L.; An, H.; Lin, W.; Tarrant, T.; Lin, W. *Angew. Chem., Int. Ed.* **2007**, *46*, 3680−3682.
(11) Lin, Y. S.; Wu, S. H.; Hung, Y.; Chou, Y. H.; Chang, C.; Lin, M. L.; Tsai, C. P.; Mou, C. Y. *Chem. Mater.* **2006**, *18*, 5170−5172.
(12) Ang, C. Y.; Giam, L.; Chan, Z. M.; Lin, A. W. H.; Gu, H. W.; Devlin, E.; Papadfthymiou, G. C.; Selvan, T. S.; Ying, J. Y. *Adv. Mater.* **2009**, *21*, 869−873.
(13) Leung, K. C.-F.; Xuan, S. H.; Lo, C.-M. *ACS Appl. Mater. Interfaces* **2009**, *1*, 2005−2012.
(14) Yang, P.; Quan, Z.; Hou, Z.; Li, C.; Kang, X.; Cheng, Z.; Lin, J. *Biomaterials* **2009**, *30*, 4786−4795.
(15) Chak, C.-P.; Xuan, S. H.; Mendes, P. M.; Yu, J. C.; Cheng, C. H. K.; Leung, K. C.-F. *ACS Nano* **2009**, *3*, 2129−2138.
(16) Si, J.; Yang, H. *Mater. Chem. Phys.* **2011**, *128*, 519−524.
(17) Gai, S.; Yang, P.; Ma, P.; Wang, D.; Li, C.; Li, X.; Niu, N.; Lin, J. *J. Mater. Chem.* **2011**, *21*, 16420−16426.
(18) Xuan, S. H.; Wang, F.; Gong, X. L.; Kong, S.-K.; Yu, J. C.; Leung, K. C.-F. *Chem. Commun.* **2011**, *47*, 2514−2516.
(19) Frey, N. A.; Peng, S.; Cheng, K.; Sun, S. H. *Chem. Soc. Rev.* **2009**, *38*, 2532−2542.
(20) Cheng, K.; Peng, S.; Xu, C. J.; Sun, S. H. *J. Am. Chem. Soc.* **2009**, *131*, 10637−10644.
(21) Lu, A. H.; Salabas, E. L.; Schuth, F. *Angew. Chem., Int. Ed.* **2007**, *46*, 1222−1244.
(22) Jeong, U. Y.; Teng, X. W.; Wang, Y.; Yang, H.; Xia, Y. N. *Adv. Mater.* **2007**, *19*, 33−60.
(23) Zhuang, J. Q.; Wu, H. M.; Yang, Y. G.; Cao, Y. C. *Angew. Chem., Int. Ed.* **2008**, *47*, 2208−2212.
(24) Bao, N.; Shen, L.; Wang, Y.; Padhan, P.; Gupta, A. *J. Am. Chem. Soc.* **2007**, *129*, 12374−12375.
(25) Deng, H.; Li, X.; Peng, Q.; Wang, X.; Chen, J.; Li, Y. *Angew. Chem., Int. Ed.* **2005**, *44*, 2782−2785.
(26) Ge, J.; Hu, Y.; Biasini, M.; Beyermann, W. P.; Yin, Y. *Angew. Chem., Int. Ed.* **2007**, *46*, 4342−4345.
(27) Liu, J.; Sun, Z. K.; Deng, Y.; Zou, Y.; Li, C.; Guo, X.; Xiong, L.; Gao, Y.; Li, F.; Zhao, D. Y. *Angew. Chem., Int. Ed.* **2009**, *48*, 5875−5879.
(28) Larsen, B. A.; Haag, M. A.; Serkova, N. J.; Shroyer, K. R.; Stoldt, C. R. *Nanotechnology* **2008**, *19*, 265102: 1−6.
(29) Xuan, S. H.; Wang, Y.-X. J.; Yu, J. C.; Leung, K. C.-F. *Chem. Mater.* **2009**, *21*, 5079−5087.
(30) Hu, F. Q.; MacRenaris, K. W.; Waters, E. A.; Schultz-Sikma, E. A.; Eckermann, A. L.; Meade, T. J. *Chem. Commun.* **2010**, *46*, 73−75.
(31) Zhao, W. R.; Gu, J. L.; Zhang, L. X.; Chen, H. R.; Shi, J. L. *J. Am. Chem. Soc.* **2005**, *127*, 8916−8917.
(32) Gai, S. L.; Yang, P. P.; Li, C. X.; Wang, W. X.; Dai, Y. L.; Niu, N.; Lin, J. *Adv. Funct. Mater.* **2010**, *20*, 1166−1172.
(33) Kim, J.; Kim, H. S.; Lee, N.; Kim, T.; Kim, H.; Yu, T.; Song, I. C.; Moon, W. K.; Hyeon, T. *Angew. Chem., Int. Ed.* **2008**, *47*, 8438−8441.
(34) Deng, Y. H.; Qi, D. W.; Deng, C. H.; Zhang, X. M.; Zhao, D. Y. *J. Am. Chem. Soc.* **2008**, *130*, 28−29.
(35) Sen, T.; Sebastianelli, A.; Bruce, I. J. *J. Am. Chem. Soc.* **2006**, *128*, 7310−7131.
(36) Deng, Y. H.; Deng, C. H.; Qi, D. W.; Liu, C.; Liu, J.; Zhang, X. M.; Zhao, D. Y. *Adv. Mater.* **2009**, *21*, 1377−1382.
(37) Li, L.; Feng, Y. J.; Li, Y. S.; Zhao, W. R.; Shi, J. L. *Angew. Chem., Int. Ed.* **2009**, *48*, 5888−5892.
(38) Zhao, W. R.; Chen, H. R.; Li, Y. S.; Li, L.; Lang, M. D.; Shi, J. L. *Adv. Funct. Mater.* **2008**, *18*, 2780−2788.
(39) Zhu, Y. F.; Kockrich, E.; Ikoma, T.; Hanagata, N.; Kaskel, S. *Chem. Mater.* **2009**, *21*, 2547−2553.
(40) Drummond, D. C.; Meyer, O.; Hong, K.; Kirpotin, D. B.; Papahadjopoulos, D. *Pharmacol. Rev.* **1999**, *51*, 691−743.
(41) Kim, J.; Lee, J. E.; Lee, J.; Yu, J. H.; Kim, B. C.; An, K.; Hwang, Y.; Shin, C. H.; Park, J. G.; Kim, J.; Hyeon, T. *J. Am. Chem. Soc.* **2006**, *128*, 688−689.
(42) Barbe, C. B.; Bartlett, J.; Kong, L.; Finnie, K.; Lin, H. Q.; Larkin, M.; Calleja, S.; Bush, A.; Calleja, G. *Adv. Mater.* **2004**, *16*, 1959−1966.
(43) Zhang, L.; Qiao, S. Z.; Jin, Y. G.; Yang, H. G.; Budihartono, S.; Stahr, F.; Yan, Z. F.; Wang, X. L.; Hao, Z. P.; Lu, G. Q. *Adv. Funct. Mater.* **2008**, *18*, 3203−3212.
(44) Leung, K. C.-F.; Nguyen, T. D.; Stoddart, J. F.; Zink, J. I. *Chem. Mater.* **2006**, *18*, 5919−5928.
(45) Lo, P.-C.; Chan, C. M. H.; Liu, J.-Y.; Fong, W.-P.; Ng, D. K. P. *J. Med. Chem.* **2007**, *50*, 2100−2107.
(46) Lo, P.-C.; Fong, W.-P.; Ng, D. K. P. *ChemMedChem* **2008**, *3*, 1110−1117.
(47) Xuan, S. H.; Wang, Y.-X. J.; Yu, J. C.; Leung, K. C.-F. *J. Mater. Chem.* **2010**, *20*, 5086−5094.
(48) Xuan, S. H.; Wang, F.; Lai, J. M. Y.; Sham, K. W. Y.; Wang, Y.-X. J.; Lee, S.-F.; Yu, J. C.; Cheng, C. H. K.; Leung, K. C.-F. *ACS Appl. Mater. Interfaces* **2011**, *3*, 237−244.
(49) Chen, Y.; Chen, H. R.; Guo, L. M.; He, Q. J.; Chen, F.; Zhou, J.; Feng, J. W.; Shi, J. L. *ACS Nano* **2010**, *4*, 529−539.
(50) Chen, D. H.; Cao, L.; Huang, F. Z.; Imperia, P.; Cheng, Y. B.; Caruso, R. A. *J. Am. Chem. Soc.* **2010**, *132*, 4438−4444.
(51) Valle-Vigon, P.; Sevilla, M.; Fuertes, A. B. *Chem. Mater.* **2010**, *22*, 2526−2533.
(52) Buchel, G.; Unger, K. K.; Matsumoto, A.; Tsutsumi, K. *Adv. Mater.* **1998**, *10*, 1036−1038.
(53) Zhao, W. R.; Lang, M. D.; Li, Y. S.; Li, L.; Shi, J. L. *J. Mater. Chem.* **2009**, *19*, 2778−2783.
(54) Ge, J.; Hu, Y.; Yin, Y. *Angew. Chem., Int. Ed.* **2007**, *46*, 7428−7431.
(55) Ge, J.; Yin, Y. *Adv. Mater.* **2008**, *20*, 3485−3491.
(56) Lindig, B. A.; Rodgers, M. A. J.; Schaap, A. P. *J. Am. Chem. Soc.* **1980**, *102*, 5590−5593.
(57) Leung, K. C.-F.; Xuan, S. H.; Zhu, X. M.; Wang, D. W.; Chak, C.-P.; Lee, S.-F.; Ho, W. K.-W.; Chung, B. C.-T. *Chem. Soc. Rev.* **2012**, *41*, 1911−1928.
(58) Wang, Y.-X. J. *Quant. Imaging Med. Surg.* **2011**, *1*, 35−40.
(59) Zhu, X. M.; Wang, Y.-X. J.; Leung, K. C.-F.; Lee, S.-F.; Zhao, F.; Wang, D.; Lai, J. M. Y.; Wan, C.; Cheng, C. H. K.; Ahuja, A. T. *Int. J. Nanomed.* **2012**, *7*, 953−964.
(60) Wang, Y.-X. J.; Quercy-Jouvet, T.; Wang, H.-H.; Li, A.-W.; Chak, C.-P.; Xuan, S. H.; Shi, L.; Wang, D.-F.; Lee, S.-F.; Leung, P.-C.; Lau, C. B. S.; Fung, K.-P.; Leung, K. C.-F. *Materials* **2011**, *4*, 703−715.
(61) Wang, H.-H.; Wang, Y.-X. J.; Leung, K. C.-F.; Au, D. W. T.; Xuan, S. H.; Chak, C.-P.; Lee, S. K. M.; Sheng, H.; Zhang, G.; Qin, L.; Griffith, J. F.; Ahuja, A. T. *Chem.—Eur. J.* **2009**, *15*, 12417−12425.
(62) Leung, K. C.-F.; Wang, Y.-X. J.; Wang, H. H.; Xuan, S. H.; Chak, C.-P.; Cheng, C. H. K. *IEEE Trans. Nanobiosci.* **2009**, *8*, 192−198.
(63) Wang, Y.-X. J.; Wang, D.; Zhu, X. M.; Zhao, F.; Leung, K. C.-F. *Quant. Imaging Med. Surg.* **2012**, *2*, 53−56.